

Received May 17, 2021, accepted July 12, 2021, date of publication July 20, 2021, date of current version July 28, 2021.

Digital Object Identifier 10.1109/ACCESS.2021.3098727

# Modeling and Simulation on Error Spreading Over Partially and Directionally Interconnected Networks of Virtual Cellular Manufacturing System

YONG YIN<sup>1,2</sup>, JIMING SA<sup>1</sup>, AND JIAN ZHOU<sup>1</sup>

<sup>1</sup>Key Laboratory of Fiber Optic Sensing Technology and Information Processing, Ministry of Education, Wuhan University of Technology, Wuhan 430070, China

<sup>2</sup>Shenzhen Research Institute, Wuhan University of Technology, Shenzhen 518000, China

Corresponding author: Jiming Sa (jimingsa@whut.edu.cn)


This work was supported in part by the National Natural Science Foundation of China under Grant 51875429, and in part by the General Program of Shenzhen Natural Science Foundation under Grant JCYJ20190809142805521.

**ABSTRACT** Networks constituting virtual cellular manufacturing system (VCMS) cells are partially interconnected while the interlinks are directional and the interlink numbers between cells are unequal, which was not considered in previous studies. In this study, a model based on susceptible–infectious–removed–susceptible was developed to analyze error spreading over an interconnected network, and theoretical analysis was performed. Based on simulations, we found the following: (i) random interlinks between subnetworks insignificantly affected the interconnected network; (ii) a large interlinking propagation efficiency raised the infection probability of the interconnected network of VCMS; (iii) the topological structures of scale-free subnetworks shaped by cells could inhibit infection propagation. Using two real cases, we verified the conclusions drawn from the error spreading model. This study provides sound foundations to optimize the structural constitution of a VCMS during its cell formation and arrangement periods.

**INDEX TERMS** VCMS, interconnected network, error spreading, SIRS.

## I. INTRODUCTION

Group technology (GT) is based on a general principle that many parts of a product have similarities in geometry, manufacturing process, or functions, and these parts can be manufactured in one location using a small number of machines or processes to save time and effort [1]. As a typical application of GT, cellular manufacturing systems (CMSs) have long been considered efficient in improving the productivity of batch production systems, exploiting part similarities [2]. The benefits of employing a CMS are attractive [3]. First, CMSs have the advantage of managing material flow easily due to part similarities and work station proximity. Second, cells induce simplified, higher validity costs since the costs of producing parts are contained within cells rather than scattered in distance. Third, cells under performing in quality can be easily traced and targeted for improvement, which facilitates both production and quality control.

The associate editor coordinating the review of this manuscript and approving it for publication was Chao Tong .

The benefits of CMSs are obvious. However, they are available only when product families are sufficiently stable and production volumes are relatively small or easy to move [4]. For instance, machines are usually duplicated to restrict the manufacturing of parts in their respective manufacturing cells, which generate an excessive production capacity and increase operational and maintenance costs. Moreover, the physical location of machines must be changed on the shop floor to reconfigure machine cells. Therefore, long times must be taken. To reduce the negative implications of a CMS while keeping its positive aspects, virtual CMS (VCMS) was proposed as an alternative [5]. The main difference between a VCMS and CMS is that the workstations in a virtual manufacturing cell are not grouped physically on the production floor but are envisaged.

In a VCMS, a product to be manufactured comprises a series of components or parts. These parts are processed by machines or equipment within different virtual cells. Machines or equipment in different virtual cells connects in different ways, such as material flows, information, and

energy connections [6]. Certain precedence constraints (part A must be manufactured before part B) and feedback constraints (processed part B may affect the original part A so that part A should be re-processed) are also inescapable. Thus, errors of one part will unavoidably cause errors in other parts through connections. With the error accumulation or stack up in all parts, error propagation may result in “avalanches” of the entire VCMS. Analyzing and handling error spreading on VCMSs can anticipate, capture, and prevent error propagations in advance; this is the first motivation of this study.

Recently, research on complex networks has become a hotspot in complexity science. Virus spreading is one of the most successful application areas of complex network theory. Here, “virus” may refer to product errors, rumors, memes, and the likes [7]. In complex networks, a virus passes from one node to another, which probably contributes to the virus spreading in a large scope, and blocks the information flow in the complex network or even paralyzes the entire network operation. Error spreading in VCMSs is similar to virus spreading in complex networks. Therefore, error spreading analysis in VCMSs can be solved by virus spreading models in complex networks; this is another motivation of this study.

As mentioned above, a VCMS involves using many virtual cells to manufacture a product. Each virtual cell comprises multiple machines or equipment accomplishing a certain number of manufacturing parts. As cells in a VCMS are “virtual”, they can be situated in or outside a workshop in many separated sites or even in different enterprises over the Internet. Parts manufactured in different individual cells are linked with each other for processing orders or material flows, and the linkage relationship constitutes a subnetwork within each cell if the parts are treated as nodes, and the linkage between nodes is regarded as edges. Subnetworks constituting different cells in a VCMS form interconnected networks.

In this study, complex network theory is employed to study error spread issues in VCMS. More specifically, the product errors in VCMS are treated as viruses and the error propagation is considered as virus spreading, so that error spreading analysis in the interconnected network of a VCMS can be solved by virus spreading models with complex network theory.

The rest of this article is organized as follows. Section 2 gives a brief review of studies on virus dynamics in complex networks. Section 3 demonstrates an interconnected network of a VCMS comprising three subnetworks. Susceptible–infectious–removed–susceptible (SIRS) virus modeling and numerical analysis on a three-layer interconnected network are employed based on an SIRS virus model. In Section 4, numerical simulations are performed to illustrate and extend analytical results. Section 5 concludes this study and gives hints for future study.

## II. BACKGROUNDS

We adopt virus spreading models with complex network theory to handle error spreading problems in this study.

In this section, we make a summarized survey on existing studies.

As a hot point in complex network theory, virus dynamics over complex networks have attracted many researchers’ attention. Compartmental models in epidemiology serving as a base mathematical framework for understanding the complex dynamics have been developed in the early 1900s [8]. The first model, namely susceptible–infectious (SI) model, was proposed as a trial of understanding the damn virus in Mumbai by dividing the population into two groups using differential equations [9]. Later, the susceptible–infectious–removed (SIR) model was proposed by Kermack and McKendrick to explain a plague and cholera virus [9]. SIR is a simple compartmental model, and many other models are derivations of it. Some popular models are SIS, SEIS, SEIR, MSIR, MSEIR, and MSEIRS (S: susceptible, I: infectious, R: removed, E: exposed in the latent period, and M: passively immune) [10].

The above mentioned studies focused on cases with a single network, although many meaningful results have been obtained. However, as many real-world networks interact with or depend on each other, these networks can be treated as multiple complex networks jointed together, which have been termed as multilayer networks, interdependent networks, interconnected networks, or network of networks. For instance, in real-world power grids, power stations need communication nodes, whereas control and communication nodes need power stations for electricity, thus the electrical grid networks are almost always coupled with communication or computer networks [11]. Other examples are transportation, manufacturing, and logistical networks [12]. Some progress has been achieved in the study of virus spreading on multilayer networks. For example, Buono *et al.* [13] studied an SIR model in partially overlapped multiplex networks. Dickison *et al.* [14] studied the dynamic behavior of SIR epidemics in interconnected networks. Buldyrev *et al.* [15] revealed that, unlike a single scale-free (SF) network, which was highly robust against epidemics, an interdependent network comprising two SF networks was vulnerable to a cascade of random failure for epidemic spreading. Funk and Jansen [16] investigated the effects of the layer overlapping in a two-layer network by extending the bond percolation analysis of two competitive viruses. Wang *et al.* [17] studied the scenario of epidemic spreading on a one-way-coupled network comprising two subnetworks; they found that the basic reproduction number  $R_0$  was independent of the cross-infection rate and cross-contact pattern, and it increased rapidly with the growth of inner infection rate if the inner contact pattern was SF. Zuzek *et al.* [18] studied random immunization in a partially overlapped multiplex network and concluded that the critical threshold of the epidemic was dominated by the most heterogeneous layer when the overlapping fraction  $q$  was very small.

Considerable progress has been made in the studies of virus dynamics over single complex and interconnected networks recently. However, many challenges still exist in

either mathematical or model aspects when these studies are employed in VCMSs for the following reasons.

(i) The links between different cells are partially interconnected, and the interconnections are directional, because one part in a cell may have a directional linking relationship of assembly or process sequence with other parts in another cell, while others have no links. Thus, the linking strengths coupling different cells are unequal. This model is different from those in [16], [17], and [19].

(ii) The types of different subnetworks shaped by different cells vary. For instance, a subnetwork formed by one cell has been affirmed as an SF network [6], whereas another has been proven as a small world (SW) network [20]. Furthermore, the numbers of nodes in each subnetwork vary since the number of parts manufactured in each cell may be unequal.

In this study, we develop a framework to model the virus spreading of interconnected networks that can be applied to the error propagation in a VCMS considering the above two properties. Each subnetwork in the model varies in type and size. Besides, subnetworks in the model are partially interconnected, and the interconnected links are directional. Analytical and numerical methods are employed to study virus spreading issues.

Notably, when a VCMS is organized for product manufacturing, the total number of parts involved in the product is kept constant. Thus, the SIRS model is more adaptable to the interconnected network of a VCMS because some error parts can be restored and some parts with severe errors are removed from the VCMS, although derived models, such as SEIR, MSIR, and MSEIR, are used more in certain virus spreading cases.

### III. MODELS AND ANALYSIS

For simplification, we assume the interconnected network of a VCMS comprises three subnetworks—A, B, and C—in our model, representing the subnetworks shaped by three cells. Two types of links exist in the interconnected network: connectivity links (also called intralinks) within each subnetwork, enabling the nodes to function cooperatively as a subnetwork, and interconnected links (also called interlinks) between subnetworks, namely, cross-links between A and B, A and C, and B and C, resulting in the error propagation of nodes in one subnetwork to those of another. Fig. 1 shows the structure of the interconnected network of a VCMS. Interlinks are directional, connecting the supporting node (i.e., node a) in one subnetwork (i.e., A) with the supported node (i.e., node b) in another (i.e., C).

We study the model of the error spreading over the interconnected network of a VCMS comprising three subnetworks, A, B, and C. Interconnected links exist between each subnetwork, which may lead to cross propagation. However, only the interlinks from infectious nodes (I) of one subnetwork (for example, A) to susceptible nodes (S) of other subnetworks (for example, B and C) may prompt cross propagation among subnetworks. The latent reason is that only infectious nodes have infectiousness and only susceptible

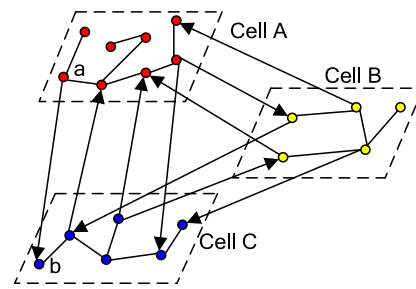


**FIGURE 1.** Illustrative structure of the interconnected network of a VCMS. Subnetworks A, B, and C are different in size and are partially interconnected. Links between different subnetworks are directional, and the linking strengths are unequal.

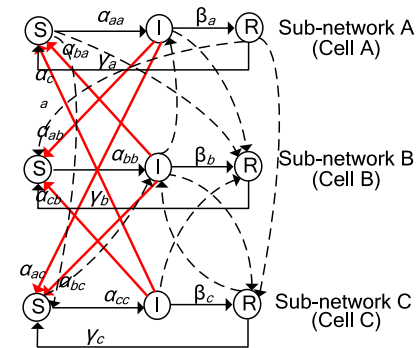


**FIGURE 2.** Demonstrative SIRS model over the interconnected network of a VCMS comprising three subnetworks, A, B, and C. Interlinks prompting cross propagation are marked with a red solid line with arrows indicating directions. The dotted lines represent interlinks from S to R, S to S, S to I, I to R, I to I, R to S, R to I, or R to R that cannot result in cross propagation.  $\alpha_{aa}$  represents the infectious probability of susceptible nodes within subnetwork A for intralinks of infected nodes;  $\alpha_{ba}$  and  $\alpha_{ca}$  express the infectious probability of susceptible nodes in subnetwork A for infections from interlinks from subnetworks B and C, respectively;  $\alpha_{bb}$ ,  $\alpha_{cc}$ ,  $\alpha_{ab}$ ,  $\alpha_{ac}$ ,  $\alpha_{bc}$ , and  $\alpha_{cb}$  have similar meanings;  $\gamma_a$  and  $\beta_a$  mean the recuperative and removal probabilities, respectively, of infected nodes in subnetwork A;  $\gamma_b$ ,  $\beta_b$ ,  $\gamma_c$  and  $\beta_c$  are similarly defined, respectively have similar meanings.

**TABLE 1.** Symbols involved in this subsection.

Symbol	Meaning
$X$	Identifier of each sub-network, $X \in (A, B, C)$
$mn$	Inter or intra linking relationship of subnetworks, $mn \in (aa, ab, ac, ba, bb, bc, ca, cb, cc)$
$(i, j, k)$	A node has $i$ links with sub-network A, $j$ links with B and $k$ links with C
$(i, )$	A node has $i$ links with sub-network A and any number of links with B or C
$(, j)$	A node has $j$ links with sub-network B and any number of links with A or C
$(, k)$	A node has $k$ links with sub-network C and any number of links with A or B
$P_X(i, j, k)$	Coupling probability of a sub-network $X$ , $X \in (A, B, C)$
$\Theta_{mn}(t)$	Probability that a randomly selected edge connects with an infectious node for $mn$ links
$k_a, k_b, k_c$	Degree of a randomly selected node within sub-network A, B, or C, respectively
$\langle k \rangle_{mn}$	Average degree for $mn$ links

nodes are susceptible to infections. Fig. 2 depicts a SIRS model of the interconnected network in such cases.

Some symbols involved are listed in Table 1.

We define  $N_A(i, j, k)$  as the number of nodes in subnetwork A that has  $i$  intra-links within its subnetwork, with  $j$  and  $k$  inter-links from subnetwork B and C, respectively. Similarly,  $N_B(i, j, k)$  and  $N_C(i, j, k)$  are defined. Thus, the coupling degree distributions of each subnetwork can be calculated as follows:

$$\begin{aligned} P_A(i, j, k) &= \frac{N_A(i, j, k)}{N_A} \\ P_B(i, j, k) &= \frac{N_B(i, j, k)}{N_B} \\ P_C(i, j, k) &= \frac{N_C(i, j, k)}{N_C}. \end{aligned} \quad (1)$$

In addition, the marginal degree distributions are given by

$$\begin{aligned} P_A(i, \cdot) &= \sum_{j=0} \sum_{k=0} P_A(i, j, k) \\ P_A(\cdot, j) &= \sum_{i=0} \sum_{k=0} P_A(i, j, k) \\ P_A(\cdot, \cdot, k) &= \sum_{i=0} \sum_{j=0} P_A(i, j, k) \\ P_B(i, \cdot) &= \sum_{j=0} \sum_{k=0} P_B(i, j, k) \\ P_B(\cdot, j) &= \sum_{i=0} \sum_{k=0} P_B(i, j, k) \\ P_B(\cdot, \cdot, k) &= \sum_{i=0} \sum_{j=0} P_B(i, j, k) \\ P_C(i, \cdot) &= \sum_{j=0} \sum_{k=0} P_C(i, j, k) \\ P_C(\cdot, j) &= \sum_{i=0} \sum_{k=0} P_C(i, j, k) \\ P_C(\cdot, \cdot, k) &= \sum_{i=0} \sum_{j=0} P_C(i, j, k). \end{aligned} \quad (2)$$

The coupling relationships among each subnetwork are expressed as follows:

$$\begin{cases} \frac{ds_{Xk}(t)}{dt} = - \sum \lambda_{mn} P_X(i, j, k) s_{Xk}(t) \Theta_{mn}(t), \\ \frac{di_{Xk}(t)}{dt} = \sum \lambda_{mn} P_X(i, j, k) s_{Xk}(t) \Theta_{mn}(t) - i_{Xk}(t), \\ \frac{dr_{Xk}(t)}{dt} = i_{Xk}(t), \end{cases} \quad (3)$$

where  $\lambda_{aa} = \alpha_{aa}/(\beta_a + \gamma_a)$ ,  $\lambda_{ba} = \alpha_{ba}/(\beta_a + \gamma_a)$ ,  $\lambda_{ca} = \alpha_{ca}/(\beta_a + \gamma_a)$ ,  $\lambda_{bb} = \alpha_{bb}/(\beta_b + \gamma_b)$ ,  $\lambda_{ab} = \alpha_{ab}/(\beta_b + \gamma_b)$ ,  $\lambda_{cb} = \alpha_{cb}/(\beta_b + \gamma_b)$ ,  $\lambda_{cc} = \alpha_{cc}/(\beta_c + \gamma_c)$ ,  $\lambda_{ac} = \alpha_{ac}/(\beta_c + \gamma_c)$ ,  $\lambda_{bc} = \alpha_{bc}/(\beta_c + \gamma_c)$ .

$\Theta_{mn}(t)$  is used in Eq. (3) to represent the probability that a randomly selected edge connects with an infectious node for  $mn$  links:

$$\begin{aligned} \Theta_{aa}(t) &= \sum_{i=0} \sum_{j=0} \sum_{k=0} \frac{(k-1)P_A(i, j, k)i_{Ak}(t)}{\langle k \rangle_{aa}} \\ \Theta_{ab}(t) &= \sum_{i=0} \sum_{j=0} \sum_{k=0} \frac{(k-1)P_A(i, j, k)i_{Ak}(t)}{\langle k \rangle_{ab}} \\ \Theta_{ac}(t) &= \sum_{i=0} \sum_{j=0} \sum_{k=0} \frac{(k-1)P_A(i, j, k)i_{Ak}(t)}{\langle k \rangle_{ac}} \\ \Theta_{bb}(t) &= \sum_{i=0} \sum_{j=0} \sum_{k=0} \frac{(k-1)P_B(i, j, k)i_{Bk}(t)}{\langle k \rangle_{bb}} \end{aligned}$$

$$\begin{aligned} \Theta_{ba}(t) &= \sum_{i=0} \sum_{j=0} \sum_{k=0} \frac{(k-1)P_B(i, j, k)i_{Bk}(t)}{\langle k \rangle_{ba}} \\ \Theta_{bc}(t) &= \sum_{i=0} \sum_{j=0} \sum_{k=0} \frac{(k-1)P_B(i, j, k)i_{Bk}(t)}{\langle k \rangle_{bc}} \\ \Theta_{cc}(t) &= \sum_{i=0} \sum_{j=0} \sum_{k=0} \frac{(k-1)P_C(i, j, k)i_{Ck}(t)}{\langle k \rangle_{cc}} \\ \Theta_{ca}(t) &= \sum_{i=0} \sum_{j=0} \sum_{k=0} \frac{(k-1)P_C(i, j, k)i_{Ck}(t)}{\langle k \rangle_{ca}} \\ \Theta_{cb}(t) &= \sum_{i=0} \sum_{j=0} \sum_{k=0} \frac{(k-1)P_C(i, j, k)i_{Ck}(t)}{\langle k \rangle_{cb}}, \end{aligned} \quad (4)$$

where

$$\begin{aligned} \langle k \rangle_{aa} &= \sum_{i=0} i P_A(i, \cdot) \\ \langle k \rangle_{ab} &= \sum_{j=0} j P_A(\cdot, j) \\ \langle k \rangle_{ac} &= \sum_{k=0} k P_A(\cdot, \cdot, k) \\ \langle k \rangle_{bb} &= \sum_{i=0} i P_B(i, \cdot) \\ \langle k \rangle_{ba} &= \sum_{j=0} j P_B(\cdot, j) \\ \langle k \rangle_{bc} &= \sum_{k=0} k P_B(\cdot, \cdot, k) \end{aligned} \quad (5)$$

Notably, as subnetworks in VCMSs are directionally and partially interconnected, the numbers of links from subnetwork A to B, B to A, A to C, and C to A are unequal; in other words, it means

$$\begin{aligned} N_A \langle k \rangle_{ba} &\neq N_B \langle k \rangle_{ab} \neq N_C \langle k \rangle_{ac} \neq N_A \langle k \rangle_{ca} \\ &\neq N_B \langle k \rangle_{cb} \neq N_C \langle k \rangle_{bc}. \end{aligned} \quad (6)$$

Using (1)–(6), we can obtain

$$\begin{cases} \frac{di_{Ak}(t)}{dt} = \lambda_{aa} P_A(i, j, k) s_{Ak}(t) \Theta_{aa}(t) \\ \quad + \lambda_{ba} P_A(i, j, k) s_{Ak}(t) \Theta_{ba}(t) \\ \quad + \lambda_{ca} P_A(i, j, k) s_{Ak}(t) \Theta_{ca}(t) - i_{Ak}(t), \\ \frac{di_{Bk}(t)}{dt} = \lambda_{bb} P_B(i, j, k) s_{Bk}(t) \Theta_{bb}(t) \\ \quad + \lambda_{ab} P_B(i, j, k) s_{Bk}(t) \Theta_{ab}(t) \\ \quad + \lambda_{cb} P_B(i, j, k) s_{Bk}(t) \Theta_{cb}(t) - i_{Bk}(t), \\ \frac{di_{Ck}(t)}{dt} = \lambda_{cc} P_C(i, j, k) s_{Ck}(t) \Theta_{cc}(t) \\ \quad + \lambda_{ac} P_C(i, j, k) s_{Ck}(t) \Theta_{ac}(t) \\ \quad + \lambda_{bc} P_C(i, j, k) s_{Ck}(t) \Theta_{bc}(t) - i_{Ck}(t). \end{cases} \quad (7)$$

Hethcote [21] defined a threshold parameter to qualify the virus transmission effectively in the SIRS model, known as the basic reproduction number  $R_0$ . If  $R_0 < 1$ , then the SIRS model is asymptotically stable, and the disease cannot invade the candidates, whereas if  $R_0 > 1$ , the SIRS model is unstable, and spreading is possible. However, the existence of the coupling relationship among each subnetwork makes  $R_0$  more complex. In this section, we employ  $R_0$  characterized as the spectral radius of the next generation matrix to determine

the linear stability of the error spreading in our model. For the SIRS model over the interconnected network of a VCMS, let

- (i)  $F$  is be the rate expressing new infections from S to I,
- (ii)  $V^+$  is be the rate of transfer of individuals from I to R,
- (iii)  $V^-$  is be the rate of transfer of individuals from R into S.

The spectral radius of the next generation matrix for the SIRS model is defined as follows [22]:

$$R_0 = \rho(FV^{-1}), \tag{8}$$

where  $V = V^- - V^+$ ;  $\rho(A)$  denotes the spectral radius of a matrix  $A$  [[23];  $A$  is a  $9 \times 9$  matrix for our model, comprising three subnetworks.

Define that

$$\zeta = \begin{bmatrix} \sum_{i=0} \sum_{j=0} \sum_{k=0} \lambda_{mn} P_A(i, j, k) s_{Ak}(t) \Theta_{mn}(t) \\ \sum_{i=0} \sum_{j=0} \sum_{k=0} \lambda_{mn} P_B(i, j, k) s_{Bk}(t) \Theta_{mn}(t) \\ \sum_{i=0} \sum_{j=0} \sum_{k=0} \lambda_{mn} P_C(i, j, k) s_{Ck}(t) \Theta_{mn}(t) \end{bmatrix},$$

$$\psi = \begin{bmatrix} i_{Ak}(t) \\ i_{Bk}(t) \\ i_{Ck}(t) \end{bmatrix}. \tag{9}$$

We have

$$F = \frac{\partial \zeta}{\partial t}$$

$$V = \frac{\partial \psi}{\partial t}. \tag{10}$$

As the coupling degree distributions of different subnetworks are independent, we have

$$P_A(i, j, k) = P_A(i, )P_A(, j)P_A(, , k)$$

$$P_B(i, j, k) = P_B(i, )P_B(, j)P_B(, , k)$$

$$P_C(i, j, k) = P_C(i, )P_C(, j)P_C(, , k). \tag{11}$$

Thus, the next generation matrix can be expressed as follows, (12) as shown at the bottom of the page.

$A$  is a  $9 \times 9$  matrix; it has nine eigenvalues and the basic reproduction number  $R_0$  is the maximum one. The method to obtain  $R_0$  can be found in [2] and [23]. Based on Perron-Frobenius theorem, we have

$$\min_{i,j} \{r_i, c_j\} \leq R_0 \leq \max_{i,j} \{r_i, c_j\}, \tag{13}$$

where  $r_i$  and  $c_j$  are the sums of the elements in the  $i^{th}$  row and  $j^{th}$  column of  $A$ . Obviously, the spectral radius of the next generation matrix  $R_0$  is determined by the virus propagation efficiency  $\lambda_{mn}$ , the average degree  $\langle k_x \rangle$ , and the degree ratio  $\langle k_{mn}^2 \rangle / \langle k_x \rangle$  of each subnetwork, where  $m \in (aa, ab, ac, ba, bb, bc, ca, cb, cc)$  and  $x \in (a, b, c)$ . When  $\lambda_{ab} = \lambda_{ba} = \lambda_{ac} = \lambda_{ca} = \lambda_{bc} = \lambda_{cb} = 0$ , we have

$$R_0 = \frac{\langle k^2 \rangle}{\langle k \rangle}. \tag{14}$$

The model agrees with the virus spreading over a single network in [9].

#### IV. SIMULATIONS AND APPLICATIONS

In this section, numerical simulations are performed to study the theoretical analysis of the error spreading model discussed in Section 3. In these simulations, an interconnected network comprising three subnetworks—A, B, and C—was constructed by a generating function defined as follows:

$$G_X(x) = \sum_{k=0}^{\infty} P_X(k)x^k, \tag{15}$$

where  $x$  is a random variable;  $P_X(k)$  is the degree distribution of subnetwork  $X (X \in (A, B, C))$ . As the types of each subnetwork shaped by different cells may vary and the numbers of nodes in each subnetwork are diverse, we generated

$$A = FV^{-1} = \begin{bmatrix} \lambda_{aa} \frac{\langle k_{aa}^2 \rangle}{\langle k_a \rangle} & \lambda_{aa} \frac{\langle k_{ba}^2 \rangle}{\langle k_a \rangle} & \lambda_{aa} \frac{\langle k_{ca}^2 \rangle}{\langle k_a \rangle} & 0 & 0 & 0 & 0 & 0 & 0 \\ 0 & 0 & 0 & \lambda_{ba} \frac{\langle k_{aa}^2 \rangle}{\langle k_b \rangle} & \lambda_{ba} \frac{\langle k_{ba}^2 \rangle}{\langle k_b \rangle} & \lambda_{ba} \frac{\langle k_{ca}^2 \rangle}{\langle k_b \rangle} & 0 & 0 & 0 \\ 0 & 0 & 0 & 0 & 0 & 0 & \lambda_{ca} \frac{\langle k_{aa}^2 \rangle}{\langle k_c \rangle} & \lambda_{ca} \frac{\langle k_{ba}^2 \rangle}{\langle k_c \rangle} & \lambda_{ca} \frac{\langle k_{ca}^2 \rangle}{\langle k_c \rangle} \\ \lambda_{ab} \frac{\langle k_{ab}^2 \rangle}{\langle k_a \rangle} & \lambda_{ab} \frac{\langle k_{bb}^2 \rangle}{\langle k_a \rangle} & \lambda_{ab} \frac{\langle k_{cb}^2 \rangle}{\langle k_a \rangle} & 0 & 0 & 0 & 0 & 0 & 0 \\ 0 & 0 & 0 & \lambda_{bb} \frac{\langle k_{ab}^2 \rangle}{\langle k_b \rangle} & \lambda_{bb} \frac{\langle k_{bb}^2 \rangle}{\langle k_b \rangle} & \lambda_{bb} \frac{\langle k_{cb}^2 \rangle}{\langle k_b \rangle} & 0 & 0 & 0 \\ 0 & 0 & 0 & 0 & 0 & 0 & \lambda_{cb} \frac{\langle k_{ab}^2 \rangle}{\langle k_c \rangle} & \lambda_{cb} \frac{\langle k_{bb}^2 \rangle}{\langle k_c \rangle} & \lambda_{cb} \frac{\langle k_{cb}^2 \rangle}{\langle k_c \rangle} \\ \lambda_{ac} \frac{\langle k_{ac}^2 \rangle}{\langle k_a \rangle} & \lambda_{ac} \frac{\langle k_{bc}^2 \rangle}{\langle k_a \rangle} & \lambda_{ac} \frac{\langle k_{cc}^2 \rangle}{\langle k_a \rangle} & 0 & 0 & 0 & 0 & 0 & 0 \\ 0 & 0 & 0 & \lambda_{bc} \frac{\langle k_{ac}^2 \rangle}{\langle k_b \rangle} & \lambda_{bc} \frac{\langle k_{bc}^2 \rangle}{\langle k_b \rangle} & \lambda_{bc} \frac{\langle k_{cc}^2 \rangle}{\langle k_b \rangle} & 0 & 0 & 0 \\ 0 & 0 & 0 & 0 & 0 & 0 & \lambda_{cc} \frac{\langle k_{ac}^2 \rangle}{\langle k_c \rangle} & \lambda_{cc} \frac{\langle k_{bc}^2 \rangle}{\langle k_c \rangle} & \lambda_{cc} \frac{\langle k_{cc}^2 \rangle}{\langle k_c \rangle} \end{bmatrix} \tag{12}$$

three different kinds of subnetworks for simulations, namely, subnetwork A as SF, subnetwork B as SW, and subnetwork C as Erdos and Rnyi (ER), with their respective degree distributions described as follows:

$$\begin{aligned}
 P_A(k) &= \frac{2m(m+1)}{k(k+1)(k+2)} \propto 2m^2k^{-3} \\
 P_B(k) &= \sum_{n=0}^{f(k,K)} C_{K/2}^n (1-p)^n p^{\frac{K}{2}-n} \frac{(pK/2)^{k-\frac{K}{2}-n}}{(k-\frac{K}{2}-n)!} e^{-pK/2} \\
 P_C(k) &= \frac{N}{k} p^k (1-p)^{N-k} \propto \frac{Ke^{-K}}{k!}.
 \end{aligned} \tag{16}$$

where  $m$  is the number of nodes with which one newly added node connects each time;  $k$  is the node degree;  $K$  is the average degree of the subnetwork;  $p$  is the probability to add an edge between two randomly selected nodes;  $f(k, K)$  is minimum one of  $k - K/2$  and  $K/2$ .

First, the effects of different intercoupling preference on the spectral radius of the next generation matrix  $R_0$  are investigated. The three subnetworks were generated according to (15) and (16) with parameters  $N_A = 1000$ ,  $m = 2$ ,  $K_A = 2$ ,  $N_B = 1500$ ,  $K_B = 2.5$  and  $N_C = 2000$ ,  $K_C = 3$ . The interlinks between subnetworks were random. For each simulation, one parameter  $\lambda_{mn}$  ( $m \neq n$ ) keeps changing from varied within 0–0.6 while others were assumed to be constant with 0 for simplifications. Simulations were implemented by Matlab programs with each result averaged over 40 realizations. The results are shown in Fig. 3.

Two conclusions can be drawn from Fig. 3:

- (i) with the increase in  $\lambda_{mn}$  ( $m \neq n$ ), the value of  $R_0$  also increases in all panels, which reveal the fact that the growth of interlinking propagation efficiency  $\lambda_{mn}$  ( $m \neq n$ ) can increase the infection probability of nodes in the interconnected network of VCMS.
- (ii)  $\lambda_{cb}$  and  $\lambda_{bc}$  have high impacts on  $R_0$  and that, which can be seen in panels (a) and (b), whereas  $\lambda_{ac}$  and  $\lambda_{ab}$  have less influence on it, as shown in panels (e) and (f). The potential reasons may be that the topological structures of SW and ER subnetworks are more vulnerable to random failures (for interlinks between subnetworks are randomly distributed), whereas that of SF subnetwork is more robust.

Next, simulations were launched to reveal how interlink patterns affected infected density. Two interlink patterns between subnetworks were studied, namely, random and SF interlinks. In other words, three subnetworks were randomly interconnected for a random interlink pattern. For an SF interlink pattern, nodes in one subnetwork have partiality for interlinks with supported nodes of higher degrees in other subnetworks. Initially, subnetworks were infected with a density of 0.2, and each simulation was averaged over 40 realizations. Simulation results are shown in Fig. 4.

From Figs. 4a and 4b, for the entire interconnected network, when  $R_0 < 1$ , infected densities for all subnetworks decreased to zero, whereas, in panels (c) and (d), the infected densities gradually increased for  $R_0 > 1$  until it approached a constant value. In both cases, the interconnected network

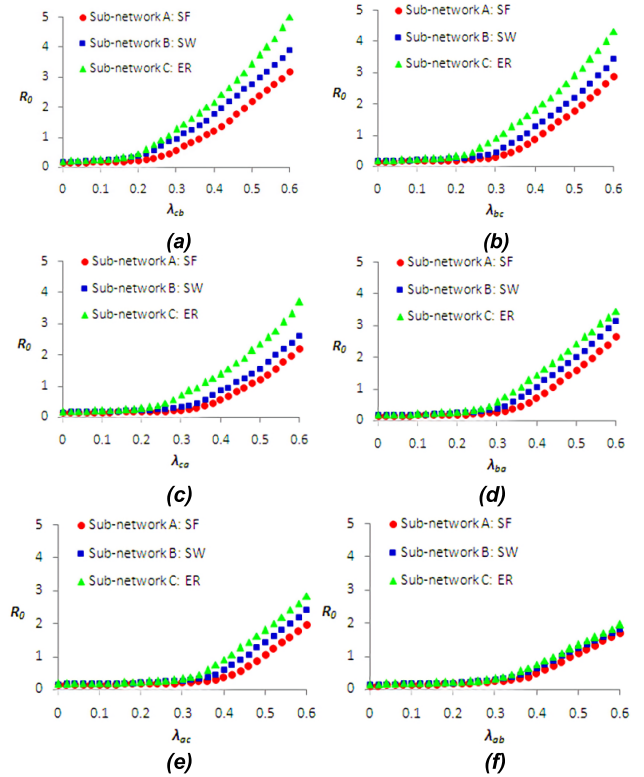


**FIGURE 3. Relationship of  $R_0$  with  $\lambda_{mn}$  for SF-SW-ER interconnected network. In all cases,  $N_A = 1000$ ,  $m = 2$ ,  $K_A = 2$ ,  $N_B = 1500$ ,  $K_B = 2.5$  and  $N_C = 2000$ ,  $K_C = 3$ : (a)  $\lambda_{ab} = \lambda_{ba} = \lambda_{ca} = \lambda_{ac} = \lambda_{bc} = 0$ ;  $\lambda_{cb}$  keeps changing from 0 to 0.6, (b)  $\lambda_{ab} = \lambda_{ba} = \lambda_{ca} = \lambda_{ac} = \lambda_{cb} = 0$ ;  $\lambda_{bc}$  keeps changing from 0 to 0.6, (c)  $\lambda_{ab} = \lambda_{ba} = \lambda_{bc} = \lambda_{ac} = \lambda_{cb} = 0$ ;  $\lambda_{ca}$  keeps changing from 0 to 0.6, (d)  $\lambda_{ab} = \lambda_{bc} = \lambda_{ca} = \lambda_{ac} = \lambda_{cb} = 0$ ;  $\lambda_{ba}$  keeps changing from 0 to 0.6, (e)  $\lambda_{ab} = \lambda_{ba} = \lambda_{ca} = \lambda_{bc} = \lambda_{cb} = 0$ ;  $\lambda_{ac}$  keeps changing from 0 to 0.6, and (f)  $\lambda_{bc} = \lambda_{ba} = \lambda_{ca} = \lambda_{ac} = \lambda_{cb} = 0$ ;  $\lambda_{ab}$  keeps changing from 0 to 0.6.**

entered a balanced state in the end. The results indicate that interlink patterns between different subnetworks cannot change the trend of infected density caused by  $R_0$ . However, when comparing panels (a) and (b), random interlinks between subnetworks insignificantly influenced the infected density of each subnetwork in panel (a), but an SF interlink pattern enhanced the decreasing speed of the infected density to zero in subnetwork A in panel (b). In panel (c), random interlinks insignificantly influenced the infected densities for all three subnetworks, whereas a SF interlink pattern facilitated the increasing process of the infected density of subnetwork A to a stable value, and the ultimate infected density value of subnetwork A became larger. The results hinted that (i) random interlinks between subnetworks had insignificant effects on the interconnected network; (ii) SF interlinks expedited the decreasing speed of the infected density to zero when  $R_0 < 1$ , whereas they promoted the cross spreading between subnetworks when  $R_0 > 1$ , speeding up the increase process of infected density to a stable but larger value.

Third, a VCMS constituting elevator manufacturing was used to investigate the proposed model and simulation results. Typically, core units of an elevator include traction, guide, car and door, electrical control, and safety protection subsystems.

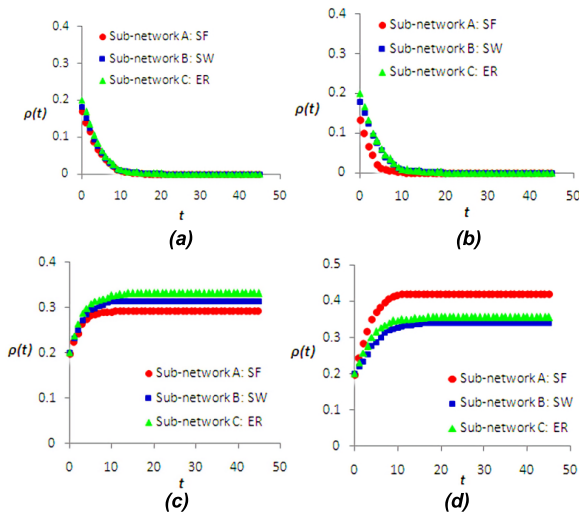


**FIGURE 4.** Effects of interlink patterns on infected density for SF-SW-ER interconnected network. In all cases,  $N_A = 1000$ ,  $m = 2$ ,  $K_A = 2$ ,  $N_B = 1500$ ,  $K_B = 2.5$  and  $N_C = 2000$ ,  $K_C = 3$ : (a)  $R_0 = 0.6$  with a random inter-link pattern, (b)  $R_0 = 0.6$  with an SF interlink pattern, (c)  $R_0 = 1.2$  with a random interlink pattern, and (d)  $R_0 = 1.2$  with an SF interlink pattern.

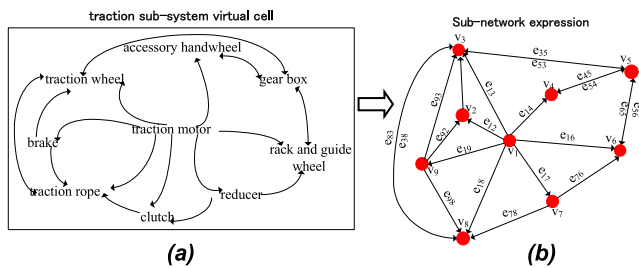


**FIGURE 5.** (a) Dependency structure of traction subsystem and (b) corresponding network expression.

These subsystems are usually manufactured in branches located in different areas with VCMSs. Further, all subsystems comprise various kinds of functional components. For example, the traction subsystem comprises traction motor, brake, clutch, gearbox, traction wheel, reducer, rack and guide wheel, traction rope and accessory handwheel, and others. The components are often manufactured in different factories. Thus, the VCMS constituted by the elevator manufacturing is an interconnected network.

Considering the traction subsystem as an example. The traction subsystem is manufactured in a virtual cell, and this virtual cell comprises multiple equipment-machining components, such as traction motor, brake, clutch, and gear box that constitute the traction subsystem. The dependency relationship of components in the traction subsystem is demonstrated in Fig. 5a, and the corresponding network expression is shown in Fig. 5b. Notably, regarding the article length, only the network expression of the traction subsystem virtual cell is described in detail. Other virtual cells, such as car and door, guide, and electrical control can be processed similarly.

When all components in different subsystem virtual cells are considered, the interconnected network expression of the entire elevator system is depicted in Fig. 6.

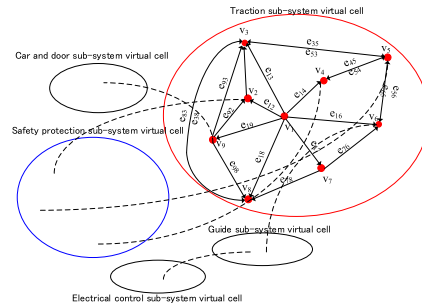


**FIGURE 6.** Interconnected network expression of the entire elevator system.

Initially, the elevator manufacturing company outsourced the subsystem manufacturing business. The virtual cells formed by subsystems are loosely linked randomly. In the economic crisis of 2008, some logistics supply chains of the downstream partners broke, which resulted in failures of some manufacturing nodes in the interconnected network. According to the models of [15] and [16], the elevator manufacturing VCMS would be damaged or even collapsed. However, the annual reports of the company revealed that the economic crisis exerted only a small influence on the elevator manufacturing VCMS. The result agreed with the conclusion from the proposed model, as the simulation on the model unveiled that random interlinks between subnetworks had insignificant effects on the interconnected network.

Later, with the expansion of the elevator company, the scale of the elevator manufacturing VCMS became larger and the spectral radius of the next generation matrix  $R_0$  kept decreasing. In 2020, the elevator company experienced a severe shortage of core components for the trade barrier. Simulation results from the model in [17] showed that the production activities of the elevator manufacturing VCMS would be totally paralyzed. However, the fact was that the elevator manufacturing VCMS returned to normal soon after a short production delay. This phenomenon agreed well with our results, which disclosed that when  $R_0 < 1$ , the SF interlinks enhanced the decreasing speed of the infected density until the network became stable. The two concrete cases verified the correctness of the proposed model.

### V. CONCLUSION

Existing studies on virus dynamics over interconnected networks are incompetent for a VCMS. In this study, a framework was developed to investigate the virus spreading issues of interconnected networks, which were similar to that constituting a VCMS considering its inherent properties. In this study, product errors were treated as viruses, and the error propagation was considered as virus spreading. Analytical methods were adopted to study the error spreading on an SF-SW-ER interconnected network based on the SIRS epidemic model. Interlinks between subnetworks of the interconnected network were directional and partial, and the numbers of links between each subnetwork were unequal. Numerical simulations were performed, and some results were obtained: (i) random interlinks between subnetworks

insignificantly affected the interconnected network; (ii) a large interlinking propagation efficiency raised the infection probability of the interconnected network of VCMS; (iii) topological structures of SF subnetworks shaped by cells could inhibit infection propagation.

The findings of this study can help optimize the constitution of the manufacturing system during cell formation and arrangement periods in the organization of a VCMS. Some potential application hints of the proposed model and the corresponding numerical simulation results are (i) a small interlinking propagation efficiency is advisable during the cell formation and arrangement periods of a VCMS; (ii) if the structure of a subnetwork constituting individual cells is SW or ER, the subnetwork size insignificantly affects the stability of the network facing errors. However, the size of a subnetwork with SF structure affects the stability of the network strongly if errors propagate; thus, small size SF subnetworks are preferable; (iii) if the spectral radius of the next generation matrix  $R_0$  is less than  $< 1$ , SF interlink patterns between cells are preferable; moreover, if  $R_0$  is larger than  $> 1$  initially, random interlink patterns are recommended because they insignificantly affect the interconnected network.

Future work following this research could continue in two aspects: (i) VCMS comprising more than three cells could be considered; (ii) more types of cells constituting different subnetworks besides SF–SW–ER should be considered.

## REFERENCES

- [1] M. Bednarek, "Group technology supporting application of lean manufacturing (LM) based on a polish case study. Measurable results and real problems," in *Proc. Int. Conf. Appl. Hum. Factors Ergonom.* Cham, Switzerland: Springer, 2018, pp. 190–200.
- [2] S. Shafiee-Gol, R. Kia, M. Kazemi, R. Tavakkoli-Moghaddam, and S. M. Darmian, "A mathematical model to design dynamic cellular manufacturing systems in multiple plants with production planning and location-allocation decisions," *Soft Comput.*, vol. 25, pp. 3931–3954, Nov. 2020.
- [3] S. Kumar, M. Gupta, M. Suhaib, and M. Asjad, "Current status, enablers and barriers of implementing cellular manufacturing system in sports industry through ISM," *Int. J. Syst. Assurance Eng. Manage.*, vol. 12, pp. 345–360, Jan. 2021.
- [4] Y. M. Méndez-Vázquez and D. A. Nembhard, "Worker-cell assignment: The impact of organizational factors on performance in cellular manufacturing systems," *Comput. Ind. Eng.*, vol. 127, pp. 1101–1114, Jan. 2019.
- [5] V. R. Kannan and S. Ghosh, "A virtual cellular manufacturing approach to batch production," *Decis. Sci.*, vol. 27, no. 3, pp. 519–539, Sep. 1996.
- [6] W. M. Han, Y. Huang, and L. Mei, "Research on virtual cellular manufacturing scheduling based on the scale-free random network model," *Appl. Mech. Mater.*, vol. 532, pp. 241–248, Feb. 2014.
- [7] T. F. Zhao, W. N. Chen, S. Kwong, T. L. Gu, H.-Q. Yuan, and J. Zhang, "Evolutionary divide-and-conquer algorithm for virus spreading control over networks," *IEEE Trans. Cybern.*, vol. 51, no. 7, pp. 3752–3766, Jul. 2021.
- [8] F. Macia-Perez, I. Lorenzo-Fonseca, and J. V. Berna-Martinez, "A formal framework for modelling complex network management systems," *J. Netw. Comput. Appl.*, vol. 40, pp. 255–269, Apr. 2014.
- [9] F. Brauer and C. Castillo-Chavez, *Mathematical Models in Population Biology and Epidemiology*. New York, NY, USA: Springer, 2001.
- [10] Y. Zhou, C. Wu, Q. Zhu, Y. Xiang, and S. W. Loke, "Rumor source detection in networks based on the SEIR model," *IEEE Access*, vol. 7, pp. 45240–45258, 2019.
- [11] M. M. Danziger, A. Bashan, Y. Berezin, L. M. Shekhtman, and S. Havlin, "An introduction to interdependent networks," in *Proc. 24th Int. Conf. Nonlinear Dyn. Electron. Syst. (NDES)*, Albena, Bulgaria, Jul. 2014, pp. 189–202.
- [12] C. Tong, Y. Lian, J. Niu, Z. Xie, and Y. Zhang, "A novel green algorithm for sampling complex networks," *J. Netw. Comput. Appl.*, vol. 59, pp. 55–62, Jan. 2016.
- [13] C. Buono, L. G. Alvarez-Zuzek, P. A. Macri, and L. A. Braunstein, "Epidemics in partially overlapped multiplex networks," *PLoS ONE*, vol. 9, no. 3, Mar. 2014, Art. no. e92200.
- [14] M. Dickison, S. Havlin, and H. E. Stanley, "Epidemics on interconnected networks," *Phys. Rev. E, Stat. Phys. Plasmas Fluids Relat. Interdiscip. Top.*, vol. 85, no. 6, pp. 1380–1404, Jun. 2012.
- [15] S. V. Buldyrev, R. Parshani, G. Paul, H. E. Stanley, and S. Havlin, "Catastrophic cascade of failures in interdependent networks," *Nature*, vol. 464, no. 7291, pp. 1025–1028, Apr. 2010.
- [16] S. Funk and V. A. A. Jansen, "Interacting epidemics on overlay networks," *Phys. Rev. E, Stat. Phys. Plasmas Fluids Relat. Interdiscip. Top.*, vol. 81, no. 3, Mar. 2010, Art. no. 036118.
- [17] L. Wang, M. Sun, S. Chen, and X. Fu, "Epidemic spreading on one-way-coupled networks," *Phys. A, Stat. Mech. Appl.*, vol. 457, pp. 280–288, Sep. 2016.
- [18] L. G. A. Zuzek, C. Buono, and L. A. Braunstein, "Epidemic spreading and immunization strategy in multiplex networks," in *Proc. J. Phys., Conf.*, 2015, vol. 640, no. 1, pp. 49–56.
- [19] Q. Wu, Y. Lou, and W. Zhu, "Epidemic outbreak for an SIS model in multiplex networks with immunization," *Math. Biosciences*, vol. 277, pp. 38–46, Jul. 2016.
- [20] Y. Wang, Z. Sun, P. Li, and Z. Zhu, "Small world and stability analysis of industrial coupling symbiosis network of ecological industrial park of oil and gas resource cities," *Energy Explor. Exploitation*, vol. 39, no. 3, pp. 853–868, May 2021.
- [21] H. W. Hethcote, "The mathematics of infectious diseases," *SIAM Rev.*, vol. 42, no. 4, pp. 599–653, 2000.
- [22] P. van den Driessche and J. Watmough, "Reproduction numbers and sub-threshold endemic equilibria for compartmental models of disease transmission," *Math. Biosci.*, vol. 180, no. 12, pp. 29–48, Nov./Dec. 2002.
- [23] O. Diekmann, J. A. P. Heesterbeek, and J. A. J. Metz, "On the definition and the computation of the basic reproduction ratio  $R_0$  in models for infectious diseases in heterogeneous populations," *J. Math. Biol.*, vol. 28, no. 4, pp. 365–382, 1990.



**YONG YIN** is currently a Professor with the Key Laboratory of Fiber Optic Sensing Technology and Information Processing, Ministry of Education, Wuhan University of Technology. His research interests include intelligent manufacturing, machine vision, and complex systems.



**JIMING SA** is currently an Associate Professor with the Key Laboratory of Fiber Optic Sensing Technology and Information Processing, Ministry of Education, Wuhan University of Technology. His research interests include intelligent manufacturing, embedded control, and complex systems.



**JIAN ZHOU** is currently a Professor with the Key Laboratory of Fiber Optic Sensing Technology and Information Processing, Ministry of Education, Wuhan University of Technology. His research interests include intelligent manufacturing, computer communication, and complex systems.

...